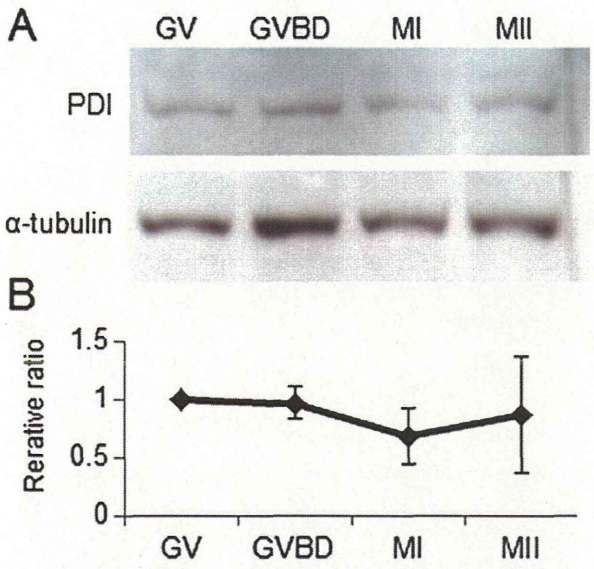

Figure 2 (A) Expression of protein disulfide isomerase (PDI) protein during maturation of porcine oocytes. PDI was detected as a single 57-kDa protein band. α-tubulin was used as an internal control. (B) Time-dependent changes of the level of PDI expression. Values indicate means ± SEM ($P < 0.05$). GV, germinal vesicle; GVBD, germinal vesicle breakdown; MI, metaphase I; MII, metaphase II.

any change in its expression level during maturation (Fig. 2). In a previous study, calreticulin, a major Ca^{2+}-binding chaperone protein, was found to be expressed at relatively higher levels in GV-stage oocytes than in MII-stage oocytes (Zhang *et al.* 2010). This suggests that certain ER proteins show quantitative increases, whereas others show quantitative decreases during nuclear progression.

PDI clusters were distributed around the first polar body at anaphase I and telophase I and after the extrusion of the first polar body, they remained there. These results suggest that PDI cluster has a function for the extrusion of the first polar body.

In a previous study, ER distribution in mouse oocytes changed in parallel to the rearrangement of the ER protein inositol 1,4,5-trisphosphate (IP3) receptor (IP3R) (Mehlmann *et al.* 1995). This protein releases Ca^{2+} from stores in the ER immediately after sperm–egg fusion; therefore, it is believed to play a role in the increased sensitivity to IP3 (FitzHarris *et al.* 2007). In bovine oocytes, IP3R was localized at the subvitelline membrane region as a diffuse and discontinuous pattern in the GV stage; however, from the MI to MII stage, IP3R was observed in the vitelline membrane cortex rather than in the animal pole (Wang *et al.* 2005).

Several studies have reported ER distribution during oocyte maturation using Ca^{2+} channels represented by IP3R (Shiraishi *et al.* 1995; Mehlmann *et al.* 1996;

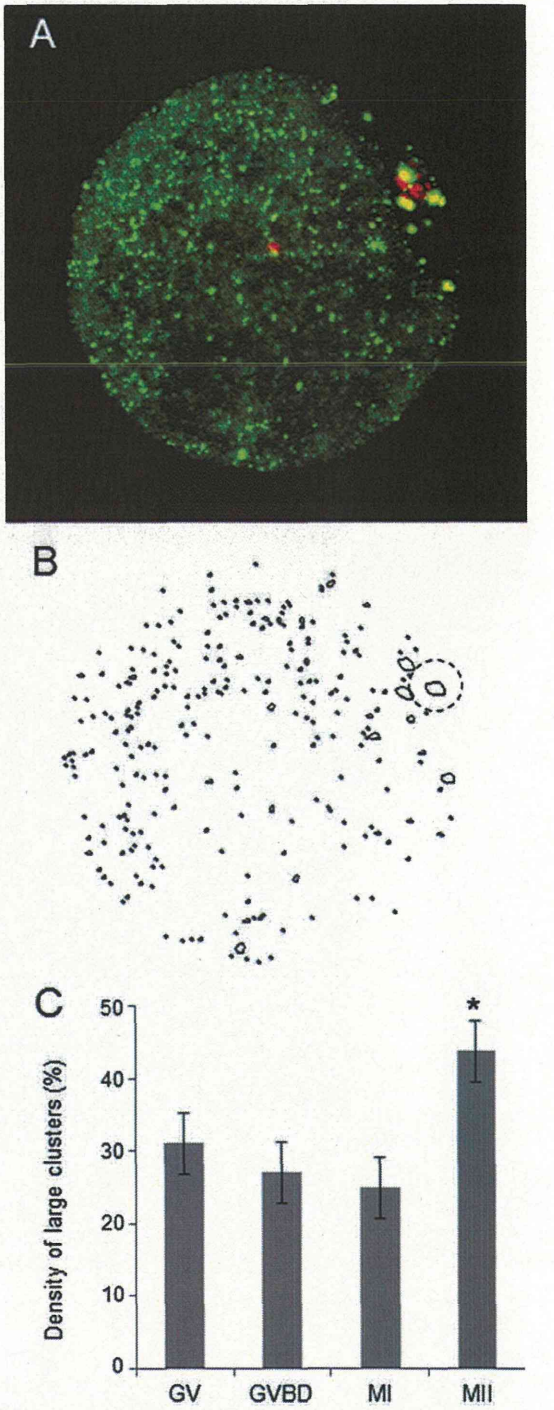

Figure 3 Density of protein disulfide isomerase (PDI) clusters during maturation of porcine oocytes. (A) Porcine metaphase II (MII)-stage oocytes. Green and red represent PDI and DNA, respectively. (B) 'Threshold' image, which makes the cluster outlines clear. The dotted frame indicates large PDI clusters (approximately 1–2 μm in diameter). (C) Density of PDI clusters. The density was calculated as the total area of 1–2 μm PDI clusters/total area of all PDI clusters. Values indicate means ± SEM ($P < 0.05$).

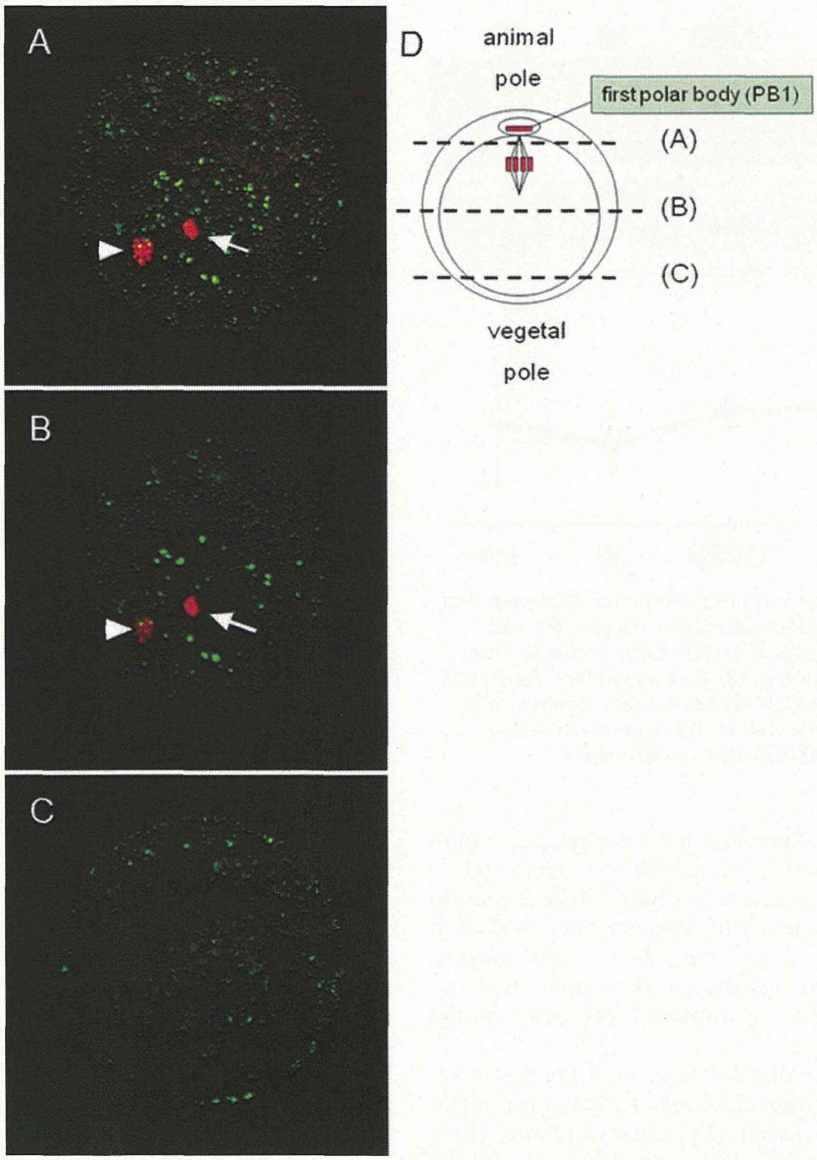

Figure 4 Position of protein disulfide isomerase (PDI) clusters in metaphase II (MII)-stage porcine oocytes matured *in vitro*. MII-stage oocytes were collected 22 h after medium replacement. The animal pole (A), equatorial (B), and the vegetal pole (C) sections are shown as the pattern diagram (D). Green and red represent PDI and DNA, respectively. The arrow indicates the first polar body, and the arrowhead indicates the metaphase plate.

Wang *et al.* 2005). In the present study, we focused on another type of ER protein – PDI. PDI is localized primarily in the ER as a luminal, peripheral membrane protein (Lambert & Freedman 1983) and is known as a major ER marker. It also plays an important role in membrane fusion. PDI has thiol isomerases on its cell surface and catalyzes thiol-disulfide exchange, which activates the fusion of proteins in membranes (Turano *et al.* 2002). Thiol-disulfide exchange is operative in gamete fusion. Gamete fusion requires a sperm surface-associated disulfide isomerase, which could then trigger a protein refolding step along the path to sperm–egg fusion (Ellerman *et al.* 2006).

Bacitracin is a membrane-impermeable PDI inhibitor that has been used over a range of concentrations in somatic cells, and it has been shown to be effective also during gamete fusion (Lahav *et al.* 2003; Markovic *et al.* 2004). When bacitracin-treated oocytes or sperm were preincubated and tested in the *in vitro* fertilization assay, the sperm showed significantly reduced fertilizing ability (Ellerman *et al.* 2006). In the

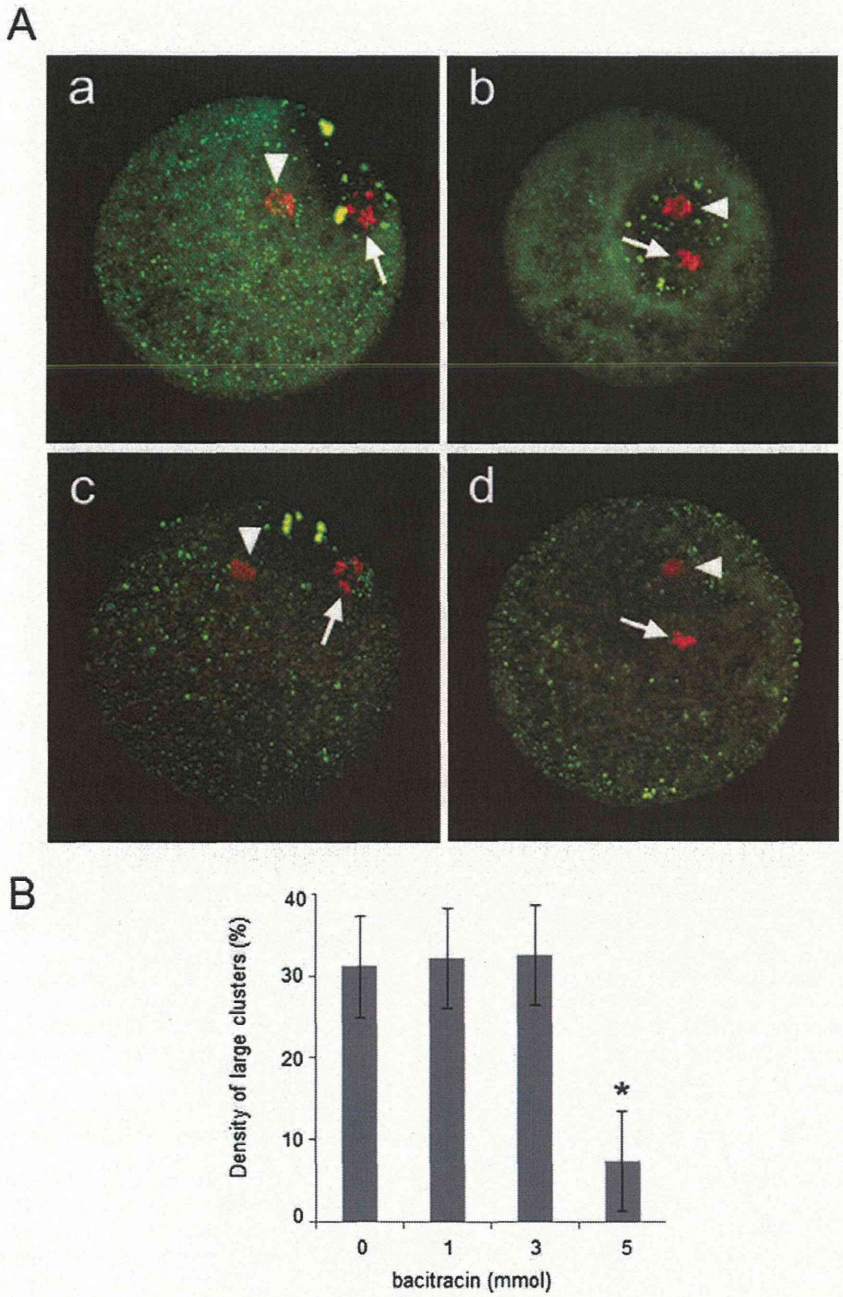

Figure 5 Effect of bacitracin on protein disulfide isomerase (PDI) clusters. After medium replacement, oocytes were cultured in the presence of different concentration of bacitracin for 22 h (A). 0 mm/moL (a), 1.0 mm/moL (b), 3.0 mm/moL (c), 5.0 mm/moL (d). (B) The density of the PDI clusters after culture in the medium containing bacitracin ($P < 0.05$).

present study, we observed that bacitracin inhibited distribution of the PDI clusters (Fig. 5). The result suggests that PDI has a function in the fertilization of the porcine oocyte. Further experiments are needed to clarify the role of PDI in oocytes for maturation, fertilization and embryo development.

Thus, we observed that, in porcine IVM oocytes, ER labeled by PDI staining form large clusters in the animal pole; this feature is specific to MII-stage porcine oocytes.

ACKNOWLEDGMENT

This work was supported by the Japan Society for the Promotion of Science Grant to E. Sato (No. 21248032).

REFERENCES

Ajduk A, Malagocki A, Maleszewski M. 2008. Cytoplasmic maturation of mammalian oocytes: development of a mechanism responsible for sperm-induced Ca^{2+} oscillations. *Reproductive Biology* **8,** 3–22.

Ellerman DA, Myles DG, Primakoff P. 2006. A role for sperm surface protein disulfide isomerase activity in gamete fusion: evidence for the participation of ERp57. *Developmental Cell* **10,** 831–837.

FitzHarris G, Marangos P, Carroll J. 2007. Changes in endoplasmic reticulum structure during mouse oocyte maturation are controlled by the cytoskeleton and cytoplasmic dynein. *Developmental Biology* **305,** 133–144.

Gilbert HF. 1998. Protein disulfide isomerase. *Methods in Enzymology* **290,** 26–50.

Jaffe LA, Terasaki M. 1994. Structural changes in the endoplasmic reticulum of starfish oocytes during meiotic maturation and fertilization. *Developmental Biology* **164,** 579–587.

Kawahara M, Mori T, Tanaka H, Shimizu H. 2002. The suppression of fragmentation by stabilization of actin filament in porcine enucleated oocytes. *Theriogenology* **58,** 1081–1095.

Lahav J, Wijnen EM, Hess O, Hamaia SW, Griffiths D, Makris M, Knight CG, Essex DW, Farndale RW. 2003. Enzymatically catalyzed disulfide exchange is required for platelet adhesion to collagen via integrin $\alpha 2\beta 1$. *Blood* **102,** 2085–2092.

Lambert N, Freedman RB. 1983. Structural properties of homogeneous protein disulphide-isomerase from bovine liver purified by a rapid high-yielding procedure. *Biochemical Journal* **213,** 225–234.

Maeda T, Yagyu T. 1997. Changes in the distribution of endoplasmic reticulum in porcine oocytes during meiotic maturation. *Journal of Mammalian Ova Reserch* **14,** 175–179.

Mann JS, Lowther KM, Mehlmann LM. 2010. Reorganization of the endoplasmic reticulum and development of Ca^{2+} release mechanisms during meiotic maturation of human oocytes. *Biology of Reproduction* **83,** 578–583.

Markovic I, Stantchev TS, Fields KH, Tiffany LJ, Tomic M, Weiss CD, Broder CC, Strebel K, Clouse KA. 2004. Thiol/disulfide exchange is a prerequisite for CXCR4-tropic HIV-1 envelope-mediated T-cell fusion during viral entry. *Blood* **103,** 1586–1594.

Mehlmann LM, Mikoshiba K, Kline D. 1996. Redistribution and increase in cortical inositol 1,4,5-trisphosphate receptors after meiotic maturation of the mouse oocyte. *Developmental Biology* **15,** 489–498.

Mehlmann LM, Terasaki M, Jaffe LA, Kline D. 1995. Reorganization of the endoplasmic reticulum during meiotic maturation of the mouse oocyte. *Developmental Biology* **170,** 607–615.

Meunier L, Usherwood YK, Chung KT, Hendershot LM. 2002. A subset of chaperones and folding enzymes form multiprotein complexes in endoplasmic reticulum to bind nascent proteins. *Molecular Biology of the Cell* **13,** 4456–4469.

Payne C, Schatten G. 2003. Golgi dynamics during meiosis are distinct from mitosis and are coupled to endoplasmic reticulum dynamics until fertilization. *Developmental Biology* **264,** 50–63.

Quinn P, Barros C, Whittingham DG. 1982. Preservation of hamster oocytes to assay the fertilizing capacity of human spermatozoa. *Journal of Reproduction and Fertility* **66,** 161–168.

Shiraishi K, Okada A, Shirakawa H, Nakanishi S, Mikoshiba K, Miyazaki S. 1995. Developmental changes in the distribution of the endoplasmic reticulum and inositol 1,4,5-trisphosphate receptors and the spatial pattern of Ca^{2+} release during maturation of hamster oocytes. *Developmental Biology* **170,** 594–606.

Stricker SA, Silva R, Smythe T. 1998. Calcium and endoplasmic reticulum dynamics during oocyte maturation and fertilization in the marine worm *Cerebratulus lacteus*. *Developmental Biology* **203,** 305–322.

Tatu U, Helenius A. 1995. Interactions between newly synthesized glycoproteins, calnexin and a network of resident chaperones in the endoplasmic reticulum. *Journal of Cell Biology* **136,** 555–565.

Terasaki M, Runft LL, Hand AR. 2001. Changes in organization of the endoplasmic reticulum during Xenopus oocyte maturation and activation. *Molecular Biology of the Cell* **12,** 1103–1116.

Turano C, Coppari S, Altieri F, Ferraro A. 2002. Proteins of the PDI family: unpredicted non-ER locations and functions. *Journal of Cell Physiology* **193,** 154–163.

Wang L, White KL, Reed WA, Campbell KD. 2005. Dynamic changes to the inositol 1,4,5-trisphosphate and ryanodine receptors during maturation of bovine oocytes. *Cloning and Stem Cells* **7,** 306–320.

Yokoo M, Miyahayashi Y, Naganuma T, Kimura N, Sasada H, Sato E. 2002. Identification of hyaluronic acid-binding proteins and their expressions in porcine cumulus-oocyte complexes during *in vitro* maturation. *Biology of Reproduction* **67,** 1165–1171.

Zhang DX, Li XP, Sun SC, Shen XH, Cui XS, Kim NH. 2010. Involvement of ER-calreticulin-Ca^{2+} signaling in the regulation of porcine oocyte meiotic maturation and maternal gene expression. *Molecular Reproduction and Development* **77,** 462–471.

Zhang JX, Braakman I, Matlack KE, Helenius A. 1997. Quality control in the secretory pathway: the role of calreticulin, calnexin and BiP in the retention of glycoproteins with C-terminal truncations. *Molecular Biology of the Cell* **8,** 1943–1954.

Theriogenology 79 (2013) 116–126

Contents lists available at SciVerse ScienceDirect

Theriogenology

journal homepage: www.theriojournal.com

Restoration of corpus luteum angiogenesis in immature hypothyroid *rdw* rats after thyroxine treatment: Morphologic and molecular evidence

Guido Macchiarelli [a,*], Maria Grazia Palmerini [a], Stefania Annarita Nottola [b], Sandra Cecconi [a], Kentaro Tanemura [c], Eimei Sato [c]

[a] *Department of Life, Health and Environmental Sciences, University of L'Aquila, L'Aquila, Italy*
[b] *Department of Anatomy, Histology, Forensic Medicine and Orthopaedics, Laboratory of Electron Microscopy "Pietro M. Motta", University La Sapienza, Rome, Italy*
[c] *Laboratory of Animal Reproduction, Graduate School of Agricultural Science, Tohoku University, Sendai 981-8555, Japan*

ARTICLE INFO

Article history:
Received 2 April 2012
Received in revised form 16 September 2012
Accepted 17 September 2012

Keywords:
Thyroxine
Angiogenesis
Corpus luteum
Pericyte
Electron microscopy
RT-PCR

ABSTRACT

Thyroxine (T4) plus gonadotropins might stimulate ovarian follicular angiogenesis in immature infertile hypothyroid *rdw* rats by upregulating mRNA expression of major angiogenic factors. Development of growing corpus luteum (CL) is strongly related to angiogenesis and to morphofunctional development of microcirculation. Our aim was to investigate if T4 is involved in CL angiogenesis and in the activation of capillary cells and angiogenic factors after ovulation in a spontaneous model of hypothyroidism, the *rdw* rat. *Rdw* rats were treated with T4 plus gonadotropins (equine chorionic gonadotropin plus human chorionic gonadotropin; eCG+hCG) or gonadotropins alone in order to evaluate the effects of T4 on early luteal angiogenesis, on microvascular cells and on expression of major growth factors which are involved in the regulation of angiogenesis. Wistar-Imamichi rats treated with gonadotropins were used as controls. The ovaries were collected 4 days after hCG administration and analyzed using morphologic and molecular approaches. Thyroxine plus gonadotropins stimulated the growth of CLs and follicles as in controls, differently from *rdw* rats treated only with gonadotropins, in which CLs were not found and only small follicles, often atretic, could be recognized. In T4 plus gonadotropin-treated *rdw* rats CLs showed increased microvasculature, numerous activated capillaries characterized by sprouting and other angiogenic figures, and associated pericytes. Quantitative analysis revealed that the number of pericytes in T4 plus gonadotropin-treated *rdw* rats was comparable with that found in control rats and was significantly higher than that found in gonadotropin-treated *rdw* rats. The mRNA expression of vascular endothelial growth factor and basic fibroblast growth factor was significantly higher in control rats and in T4 plus gonadotropin-treated *rdw* rats than in gonadotropin-treated *rdw* rats. mRNA expression of tumor necrosis factor α, transforming growth factor β, and epidermal growth factor did not show significant changes. Our data originally demonstrated that T4 promoted the growth of an active microcirculation in developing CLs of gonadotropin-primed hypothyroid *rdw* rats, mainly by inducing sprouting angiogenesis, pericyte recruitment, and upregulation of mRNA expression of vascular endothelial growth factor and basic fibroblast growth factor. In conclusion, we suggest that T4 plays a key role in restoring luteal angiogenesis in ovaries of immature hypothyroid *rdw* rats.

1. Introduction

Folliculogenesis, ovulation, and corpus luteum (CL) formation are cyclically related to phenomena of microvascular growth, remodeling and regression of blood vessels, and therefore to specific functional changes of the ovarian microcirculation. All these adaptations are fundamental to ensure fertility and normal ovarian function [1–5].

Angiogenic remodeling is particularly intense after ovulation, when new vessels develop from the pre-existing

* Corresponding author. Tel.: +39 0862433652; fax: +39 0862433785.
E-mail address: gmacchiarelli@cc.univaq.it (G. Macchiarelli).

0093-691X/$ – see front matter © 2013 Elsevier Inc. All rights reserved.
http://dx.doi.org/10.1016/j.theriogenology.2012.09.016

thecal vasculature to sustain the development of the initial CL [6–12]. CL is a highly vascularized structure that receives the greatest blood flow per unit of tissue of any organ in the body [12]. As a consequence, the rate of tissue growth and cell proliferation in growing CLs is equal to or even greater than that of the most rapidly growing and dangerous tumors [13]. Pericytes represent a large proportion of proliferating cells in growing CLs [14] and they act as guiding structures aiding the outgrowth of endothelial cells during luteal development [15]. The CL development and functionality is also ensured by the release into luteal cells of intercellular vesicles—secreted by vascular pericytes—containing a high quantity of Thy-1^+ differentiation protein, a morphoregulatory molecule associated with cell differentiation [16].

The angiogenic process is finely regulated by several hormones and growth factors that act as either stimulatory or inhibitory factors [2,3]. In the mammalian ovary, the main regulators of angiogenesis are represented by gonadotropins (follicle [FL] stimulating hormone [FSH] and luteinizing hormone [LH]) and several angiogenic factors including vascular endothelial growth factor (VEGF) [17,18]. The ovary locally produces several other growth factors with angiogenic properties such as: transforming growth factor β (TGFβ) epidermal growth factor (EGF) and tumor necrosis factor (TNF)-α [17]. Recent findings demonstrated that the thyroid hormone, thyroxine (T4), also plays a key role in ovarian FL angiogenesis [19]. It is well known that hypothyroidism is associated with infertility problems, ranging from anovulatory cycles, and sterility to abortion in many mammals and humans [20–22]. Such anomalies could be partially or totally restored by T4 administration [23] or by a combined therapy with T4 including gonadotropins, as reported in hypothyroid women [21] and in a well established model of congenital hypothyroidism, the *rdw* rat [19,24,25].

Numerous studies highlighted that T4 is actively involved in coronary and brain angiogenesis [26–28]. The mechanism of thyroid hormone-induced angiogenesis is initiated with integrin αVβ3 receptor [29] after T4 binding and involves the secretion of basic fibroblast growth factor (bFGF) and VEGF by endothelial cells, as recently reviewed [30]. In the ovary of immature female *rdw* rats, T4 markedly improved the development of follicular microvasculature, especially in the presence of eCG, by regulating the gene expression of some growth factors involved in the regulation of angiogenesis, such as VEGF, TNFα, bFGF, and of their receptors [19]. However, although it was demonstrated that T4 therapy supports the formation of functional CL and the establishment of normal pregnancy in hypothyroid rodents [31], the effect of this hormone on ovarian luteal angiogenesis has not yet been addressed.

In this study we tested the hypothesis that T4 might mediate the development of CL microcirculation in immature infertile hypothyroid *rdw* rat ovaries and mRNA expression levels of main ovarian angiogenic growth factors such as VEGF, TGFβ-1, bFGF, EGF, and TNFα.

To this aim, we performed: (1) a structural and ultrastructural study by light microscopy (LM), transmission electron microscopy (TEM), and scanning electron microscopy (SEM) of vascular corrosion casts (vcc) to analyze the ovarian microvasculature, evaluated especially in terms of capillary activation and pericyte recruitment [1,4,19]; (2) a quantitative analysis to determine the number of pericytes in follicular and luteal capillaries [5]; (3) a semiquantitative reverse-transcriptase polymerase chain reaction (RT-PCR) to analyze the mRNA expression of VEGF, TGFβ-1, bFGF, EGF, and TNFα, all involved in gonadotropin-stimulated luteal angiogenesis [2,3,13,19,32].

2. Materials and methods

2.1. Animals

Infertile immature hypothyroid *rdw* rats (N = 12; six per each experimental group), and their normal littermates (Wistar-Imamichi rats; [control] N = 4) were used. Animals were produced and maintained as previously described [19,24,25,31]. The *rdw* mutants were distinguished according to low body weight, retarded development of ears, and small body size at approximately 2 weeks of age. This study conformed to the Ethics Committee for Care and Use of Laboratory Animals for Biomedical Research of the Faculty of Agricultural Sciences, Tohoku University, Japan and to the E.C. regulation on this matter.

2.2. Experimental groups and hormonal treatments

Group 1 included Wistar-Imamichi rats, treated with eCG and hCG to induce superovulation and CL formation, used as control rats. Female immature *rdw* rats were divided randomly and treated as follows [24]: group 2, eCG and hCG; group 3, T4 and eCG and hCG.

eCG (10 IU) (Sankyo Kabu Company, Tokyo) was injected subcutaneously on Day 28 after birth; hCG (10 IU) (Sankyo Kabu Company, Tokyo) was given intraperitoneally (ip) 54 hours after eCG administration. Thyroxine (L-thyroxine, Sigma Chemical Company, St. Louis, MO, USA) was administered intraperitoneally (ip) once a day at a dose of 10 mg per 100 g of body weight, from Day 21 to Day 30 [19]. Thyroxine was dissolved in 2 mol NaOH and prepared in physiological saline solution (pH 8.3). The animals were sacrificed 4 days after hCG administration to study CL angiogenesis in the period of maximal expression (i.e., in the developing CL).

2.3. Experimental design

2.3.1. Morphologic study

2.3.1.1. Light microscopy and TEM. To assess the cellular morphologic changes of CL formation and ovarian microvasculature, LM (in semithin sections) and TEM (in ultrathin sections) studies were conducted as described previously [4,5,19]. Budding and sprouting (activated) capillaries were considered proliferative (angiogenic), and regular capillaries were considered quiescent. Proliferating and quiescent capillaries were classified on the basis of the whole capillary vessel ultrastructure, giving a special attention to the endothelial cell morphology (shape, plasma membrane specialization, nucleus morphology, and cytoplasmic

organelle amount). Capillary lumen restriction (pocket-like lumen), as well as the occurrence of capillary buds and sprouts were considered a morphologic feature of sprouting angiogenesis [4,5].

2.3.1.2. Scanning electron microscopy of vcc. CL microvascular architecture and the distribution of angiogenic and angioregressive figures were evaluated by SEM of vcc. Vessels were classified according to their diameter and shape [4,6–9]. Budding, sprouting, and splitting of capillaries from pre-existing blood vessels were considered proliferative (angiogenic) figures [5–8,33]. Incompletely filled or thin capillaries were considered degenerative figures [4,7,34].

2.3.2. Quantitative study of pericytes

Approximately sixty cross-sectioned capillaries, formed by three or fewer endothelial cells and not surrounded by vascular smooth muscle, were selected from semithin sections obtained from at least five different CLs and/or FLs of two control and eight *rdw* rats [35]. Capillaries of FLs were counted in morphologically healthy theca layers of antral to mature FLs. Interstitial (stromal) capillaries were excluded from the evaluation. Pericytes were distinguished from other cell types and enumerated according to morphologic features (shape, presence of cellular processes) and spatial distribution around the outer endothelial cell membrane. The number of capillaries and pericytes from FLs and CLs was summed to obtain the total number in the so called "follicular-luteal complex" [36], because it is from the invasion of thecal capillaries into the avascular antral cavity from which the subsequent luteal structure is originated. The Image J software (National Institutes of Health, Bethesda, MD, USA) was used to estimate the medium number of pericytes (mural cells) in each counted capillary.

2.3.3. Molecular study

mRNA expression levels of the following growth factors which are involved in the regulation of angiogenesis: VEGF, TGFβ-1, bFGF, EGF, and TNFα, were determined in *rdw* rats by RT-PCR and compared with those of control rats as previously reported [19].

2.4. Animal preparation and sample processing

Perfusion of rats (N = 8 *rdw* and N = 2 control rats) was carried out as previously described [6–8]. Briefly, animals were anesthetized with 50 mg/kg body weight ip pentobarbital sodium (50 mg/mL). The aorta was cannulated and a physiological saline solution containing heparin and 1% glutaraldehyde was allowed to flow into it. At the same time, the inferior vena cava was cut to allow the drainage of blood.

2.5. Light microscopy and TEM methods

After perfusion, one ovary per each animal was promptly fixed in 2.5% glutaraldehyde, postfixed with 1% osmium tetroxide, dehydrated in a graded ethanol series, and embedded in Agar resin as previously reported [19,36]. Sections were cut with Ultracut E-Reichert-Jung ultramicrotome. For LM, 1 μm-thick sections of the embedded tissues were stained with aqueous methylene blue, examined, and photographed with a Zeiss Ultraphot II microscope. For TEM observations, ultrathin sections of 0.11 to 0.13 μm in thickness were prepared on unsupported copper grids and stained with uranyl acetate and lead citrate. Specimens were observed and photographed with a Zeiss EM 10A microscope.

2.6. Scanning electron microscopy of vcc method

After perfusion, Mercox resin (Okenshoji Co. Ltd., Tokyo, Japan) was slowly injected into the aorta until polymerization started [19,37]. The casted ovaries (N = 1 per each animal) were removed and placed in a warm water bath to complete polymerization, corroded in a 10% NaOH solution at 60 °C for 24 to 48 hours, and gently washed for 2 to 3 hours under tap water. Then, samples were immersed in distilled water for 2 to 3 days at 60 °C to completely remove macerated tissues, and washed again under running tap water. Half of the samples were frozen at −18 °C and cut with a cooled razor blade, to allow the visualization of the internal structures of the casts. All samples were air dried, mounted on aluminum stubs and coated with platinum in an Emitech cold sputter coater at 20 mA for 2.5 minutes [6–8]. The observations were performed at low accelerating voltage (3–7 kV), in FE Hitachi S-4000 and S-4200 Field Emission Scanning Electron Microscopes.

2.7. Semiquantitative RT-PCR assay

Four days after hCG administration (postnatal day 34), the ovaries were collected from two animals from each experimental group and rapidly frozen in liquid nitrogen and then stored at −80 °C until assay. The semiquantitative

Table 1
Quantitative study of pericytes.

	Group 1		Group 2		Group 3	
	FLs	CLs	FLs	CLs	FLs	CLs
FLs/CLs evaluated	3	3	5	-	3	3
Capillaries	20 ± 3	19.3 ± 3.2	19.2 ± 1.9	-	19.7 ± 2.1	20 ± 3.6
Total capillaries	19.7 ± 2.8		19.2 ± 1.9		19.8 ± 2.6	
Pericytes	12.7 ± 1.5[a]	14 ± 1[b]	8.2 ± 1.3[c]	-	13 ± 2.6[a]	14.7 ± 1.2[b]
Total pericytes	13.3 ± 1.4[a]		8.2 ± 1.3[c]		13.8 ± 2[a]	

Data are shown as N and mean ± SD. Approximately 60 cross-sectioned capillaries, formed by three or fewer endothelial cells, were selected from semithin sections obtained from at least five different corpora lutea (CLs) and/or follicles (FLs) of two control and eight *rdw* rats. Different superscript letters indicate significant differences among experimental groups ($P < 0.001$).

RT-PCR assay was done as previously described on whole frozen ovaries [19]. Briefly, total cellular RNA was extracted from each frozen specimen with RNeasy Mini Kit (Qiagen K.K., Tokyo, Japan), treated with DNase I on RNeasy Mini Spin Columns to avoid DNA contamination. RNA was quantified using an ultraviolet-visible recording spectrophotometer (UV-160, Shimadzu Corporation, Tokyo, Japan). Semiquantitative RT-PCR was performed using Ready To Go RT-PCR Beads (Amersham Pharmacia Biotech, Inc., Piscataway, NJ, USA). One microgram of total RNA per sample was reverse transcribed by one-step protocol according to manufacturer's instructions. The RT reaction was carried out at 42 °C for 15 minutes, and samples were incubated for reaction at 95 °C for 5 minutes to inactivate the reverse transcriptase and to completely denature the template. Primer pairs for VEGF, TGFβ-1, bFGF, EGF, TNFα, and for 18S (488 base pairs) were used (Ambion Inc., Austin, TX, USA) [19]. The amplification cycle consisted of 95 °C for 1 minute, 60 °C for 1 minute, and 72 °C for 2 minutes. After 30 cycles of amplification, each PCR product was electrophoresed in a 2% agarose gel for approximately 35 minutes. The gels were stained in 1% EtBr for 45 min and pictures were taken. The bands were quantified by densitometry using NIH Image 1.63 analysis program (National Institutes of Health). Each gene mRNA level was normalized against its respective 18S mRNA and expressed as fold difference.

2.8. Statistical analysis

Quantitative data in Table 1 and semiquantitative RT-PCR data were analyzed by one way ANOVA followed by Tukey's multiple comparison test as a post test (GraphPad Prism 6). Differences with $P < 0.05$ were considered statistically significant.

3. Results

3.1. Morphological study

3.1.1. Group 1: Gonadotropin-treated Wistar-Imamichi rats (control)

By LM, control rats presented numerous FLs at different stages of growth and a few CLs (Fig. 1A). Developing CLs presented clusters of luteal cells characterized by cytoplasmic lipid droplets and interspersed in a richly vascularized connective tissue (Fig. 1A). Numerous follicular and luteal capillaries, as well as venules and arterioles of various caliber were found. The capillaries were mainly rounded, composed of 2 to 3 endothelial cells, surrounded by some pericytes (Fig. 1A, inset).

By TEM, endothelial cells of luteal capillaries showed an irregular luminal surface with numerous luminal thin and short projections, a cytoplasm with a few organelles and irregularly shaped nuclei. The capillary pericytes were provided with thin and long extensions that surrounded the endothelial cells and by round or ovoid nuclei (Fig. 2A). Endothelial cells of arterioles and venules were polyhedral, with irregularly shaped nuclei, and numerous luminal and abluminal thin, short cytoplasmic processes (Fig. 3A, B). By SEM of vcc four to six vascular plexuses (VPs) were identified on the ovarian surface of control rats. CLs showed

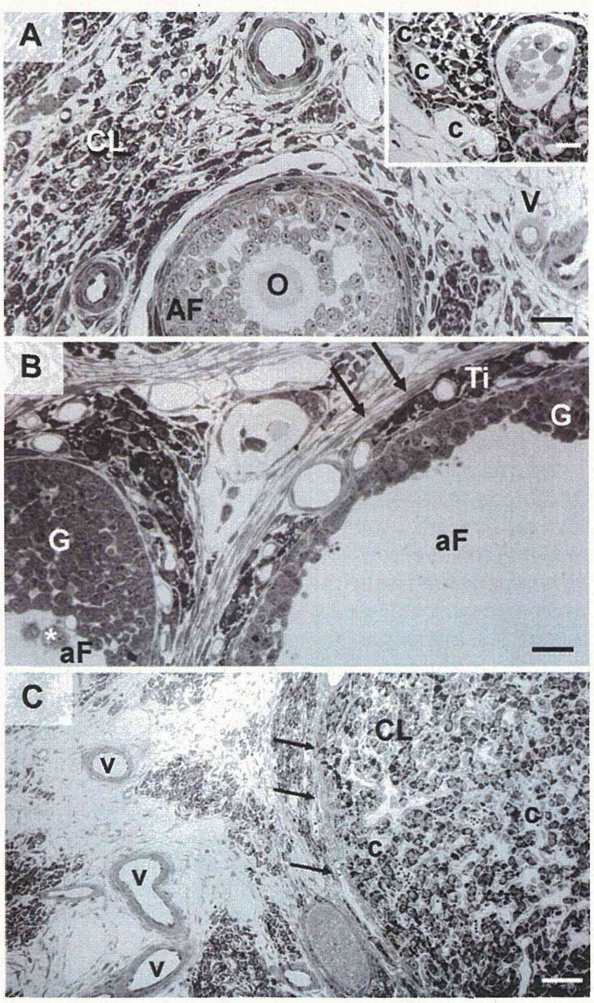

Fig. 1. Representative images of the rat ovarian cortex by light microscopy. (A) Group 1: gonadotropin-treated Wistar-Imamichi rats (control). A healthy antral follicle (AF) with the enclosed oocytes (O) is shown. The cortex is supplied by numerous stromal vessels (v) interspersed in the connective tissue. A richly vascularized developing CL, partially sectioned, is also visible. Bar, 50 μm. (Inset) A higher magnification of a developing CL. The luteal tissue is composed of clusters of luteal cells with a granular cytoplasm rich in lipid droplets, and it is highly vascularized. c, capillaries. Bar, 50 μm. (B) Group 2: gonadotropin-treated *rdw* rats. Atretic antral follicles (aF) with fluctuant granulosa cells into the follicular antrum (asterisk). An irregular circular profile characterizes these follicles. Note that the degenerative processes involve both granulosa cells (G) (follicle wall irregular in shape and thickness) and the theca layers, that appear thin and disorganized. TI, theca *interna*. Arrows indicate theca *externa*. Bar, 100 μm. (C) Group 3: Thyroxine plus gonadotropin-treated *rdw* rats. A richly vascularized corpus luteum (CL), as evidenced by numerous capillaries (c). Stromal veins (v) drained the blood flow outside the capsule of connective tissue (arrows) surrounding the CL. Bar, 100 μm.

a dense vascular network made of small caliber capillaries growing toward the antral cavity (Fig. 4A).

3.1.2. Group 2: Gonadotropin-treated rdw rats

By LM, numerous atretic antral FLs and some healthy antral FLs were seen (Fig. 1B). CLs were not found. Atretic antral FLs appeared irregularly shaped and encircled by irregular theca layers (Fig. 1B). Different to group 1, the boundary line between theca *interna* and theca *externa*

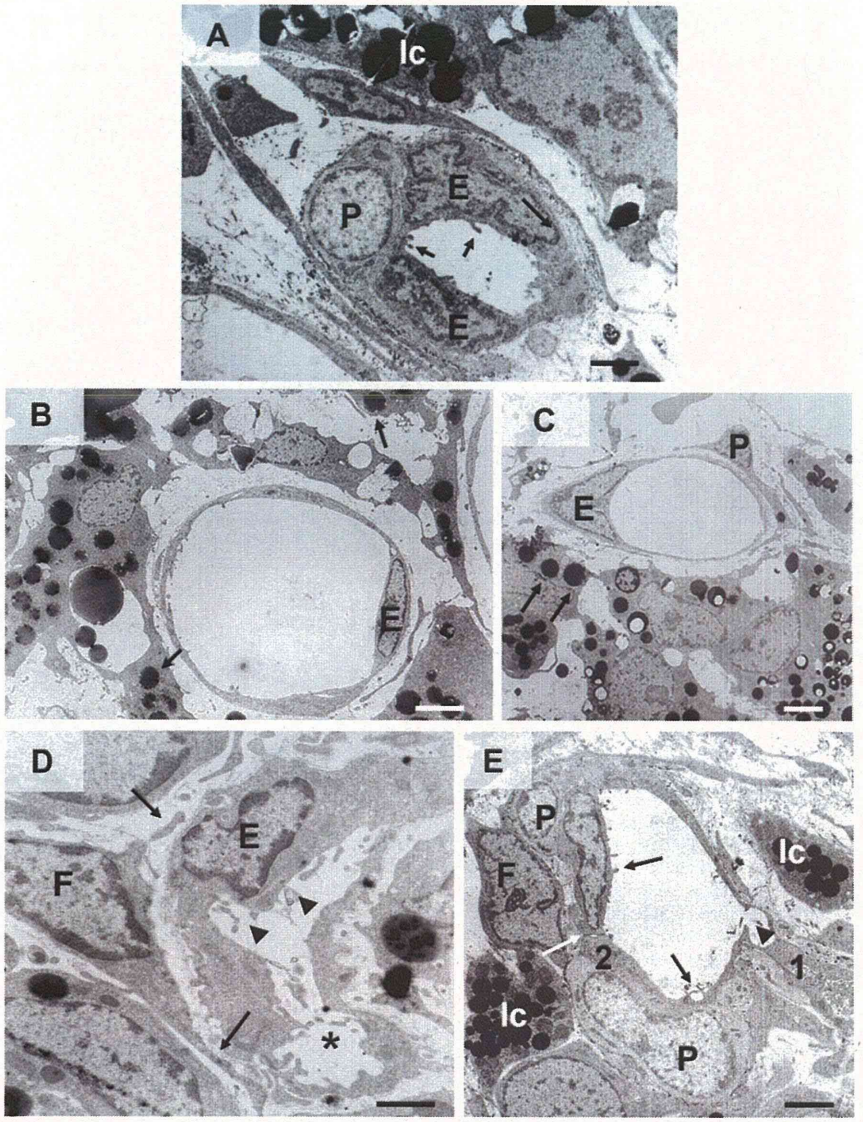

Fig. 2. Representative images of rat ovarian capillaries by transmission electron microscopy. (A) Group 1: gonadotropin-treated Wistar-Imamichi rats (control). A luteal capillary showing signs of angiogenic activation is shown. Endothelial cells (E) present irregular cytoplasmic protrusions (arrows) in the luminal surface of the plasma membrane. A pericyte (P) envelops endothelial cells with its protrusions within the microvascular basement membrane of the capillary. Luteal cells (lc) are also visible in the section. Bar, 5 μm. (B) and (C) Group 2: gonadotropin-treated *rdw* rats. Quiescent capillaries in the theca *interna* of atretic follicles. (B) The capillary shows a roundish and regular profile in section. Endothelial cells (E) are thin and flat. Bar, 5 μm. (C) a small pericyte (P) is in close proximity to the capillary and partially envelops the endothelial cell (E) with its cytoplasmic protrusions. Arrows: thecal cells showing signs of luteinization, as indicated by the accumulation of electron-dense lipid droplets in the cytoplasm. Bar, 5 μm. (D) and (E) Group 3: Thyroxine plus gonadotropin-treated *rdw* rats. Activated capillaries in developing CLs. (D) An endothelial cell (E) shows luminal cytoplasmic processes (arrowheads). A fibrocyte (F) adheres to the capillary with its long cytoplasmic processes (arrows). Note the presence of a capillary bud (asterisk). Bar, 5 μm. (E) Group 3: Thyroxine plus gonadotropin-treated *rdw* rats. A sprouting capillary in the CL. Two endothelial cells (1 and 2) show thin projections in the lumen (arrows). One of these endothelial cells (nucleus not included in the section) leads the sprout formation and the secondary lumen (arrowhead) organization. The other one is located at the beginning of the sprout. A tight junctions (white arrow) connects two endothelial cells. Note the presence of two pericytes (P) that closely envelope endothelial cells. F, fibrocyte; lc, luteal cells. Bar, 5 μm.

was hardly recognizable. Degenerative processes involved both granulosa and thecal cells. Capillary vessels were seen in the thin (15–25 μm) theca *interna*. They showed a round shape with a regular profile. Arterioles and venules were recognized in the thecal layer (Fig. 1B). Transmission electron microscopy showed thecal capillaries, characterized by a regularly shaped round or oval lumen in cross-section (Fig. 2B). As in control rats, endothelial cells were flat and provided with a smooth plasma membrane, and oval regular nuclei with substantial heterochromatin (Fig. 2B). Differently, rare pericytes with short cytoplasmic extensions were observed around some capillaries (Fig. 2C). Thecal cells with signs of luteinization (mainly represented by an increased number of lipid droplets and cytoplasmic-nuclear ratio) were found after hCG administration (Fig. 2B, C). Scanning electron microscopy of gonadotropin-treated *rdw* rat ovaries did not present microvascular casts of CLs.

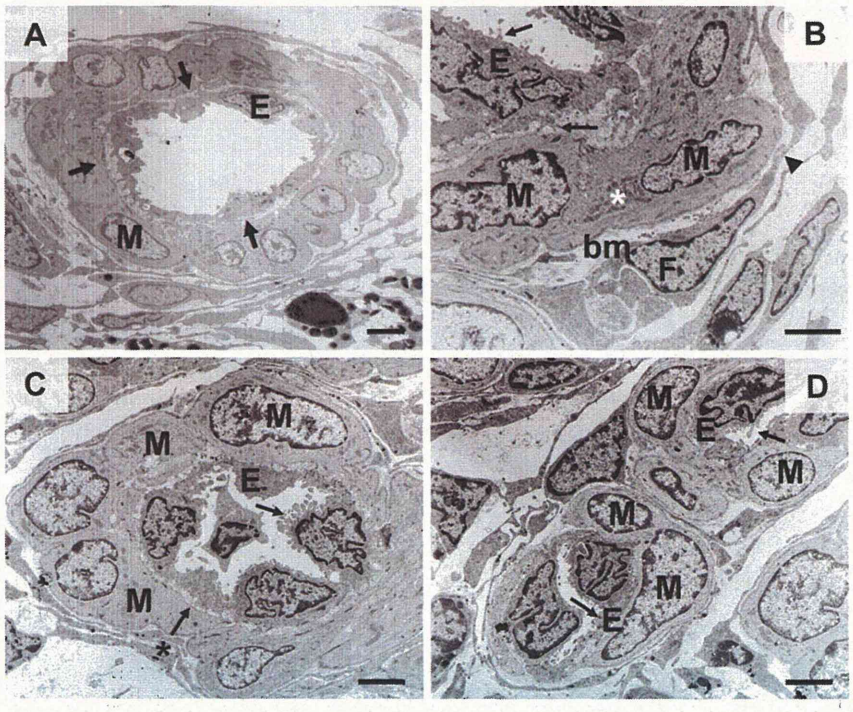

Fig. 3. Representative image of arterioles and venules, showing signs of angiogenic activation, in rat developing CLs. (A) Group 1: gonadotropin-treated Wistar-Imamichi rats (control): an arteriole. Round and swollen smooth muscle cells (M), whose nuclei are rich in heterochromatin, are separated from the adjacent luminal endothelial cells (E) by a subendothelial lamina (arrows). Note the irregular and abundant luminal cytoplasmic protrusions of endothelial cells. Bar, 5 μm. (B) Group 1: gonadotropin-treated Wistar-Imamichi rats (control): a venule. The wall of the venule, partially sectioned, shows numerous luminal and abluminal villous-like processes (arrows) of the endothelial cells (E). The smooth muscle cell (M) cytoplasm is abundant and rich in organelles (asterisk). A fibrocyte-like cell (F), with a regular nucleus, envelops with its protrusions (arrowheads) the smooth muscle cells outside the basement membrane (bm). Bar, 5 μm. (C) Group 3: thyroxine plus gonadotropin-treated *rdw* rats: an arteriole. Numerous cytoplasmic processes are present in the luminal surface of the endothelial plasma membrane (arrow). The endothelial cell nuclei show an irregular profile. The endothelial cell (E) lay down on a subendothelial lamina (asterisk plus arrow). Note the general hypertrophic aspect of the microvessels (in particular those of smooth muscle cells, M). F, fibrocytes. Bar, 5 μm. (D) Group 3: thyroxine plus gonadotropin-treated *rdw* rats: two venules. Cytoplasmic processes (arrows) protrude to the lumen of the venules. Endothelial cell (E) nuclei, polyhedral in shape and with an irregular profile, occupy a large amount of the cytoplasm. Smooth muscle cells (M) appear swollen and disposed in a single layer. Bar, 5 μm.

3.1.3. Group 3: T4 plus gonadotropin-treated rdw rats

Light microscopy of group 3 ovaries showed several developing CLs (Fig. 1C) together with healthy and atretic antral FLs. A thin capsule of connective tissue, in which arterioles and venules were recognized, encircled the CLs. Luteal cells, organized in clusters of few elements (between three and 10 cells), were immersed in a fine net of connective tissue containing numerous capillaries, similar to that observed in group 1. CL cell cytoplasm contained many lipid droplets (Fig. 1C). By TEM, luteal capillaries showed frank morphologic signs of activation such as flat or pocket-like lumen sometimes with a sinusoidal profile, thick heteromorphic endothelial cells with irregularly shaped nuclei, and numerous processes in both luminal and stromal sides of their plasma membrane (Fig. 2D, E). Endothelial cells adhered to each other through intact tight junctions (Fig. 2E). Different to group 2, most capillaries appeared activated as demonstrated by irregular luminal and abluminal cytoplasmic protrusions of different thickness and size, increase in the chromatin density, irregular basement membrane, sprouting, and budding. Several pericytes were always observed in proximity of activated capillaries (Fig. 2E, Table 1). Often, in correspondence of endothelial sprout origin, pericytes embraced and accompanied sprout formation with several cytoplasmic processes (Fig. 2E). Pericyte nuclei were round and rarely lobulated (Fig. 2E). Sometimes, stromal fibrocyte-like cells (e.g., quiescent fibroblasts characterized by a large nucleus, thin, flattened cytoplasm, and not actively secreting collagen fibers) were seen close to activated capillaries. These cells were distinguished by pericytes for their position, outside of the vascular basal membrane and were provided with long cytoplasmic processes that surrounded capillaries (Fig. 2D, E).

In CL, numerous small arterioles and postcapillary venules were seen (Fig. 3C, D). These vessels showed polyhedral, thick endothelial cells, provided with irregularly shaped nuclei and very numerous microvillous-like processes. A dense subendothelial lamina was present. Perivascular smooth muscle cells, generally monolayered, were voluminous, provided with an oval central nucleus, and normally distributed cytoplasmic organelles (Fig. 3C, D). By SEM of vcc, the surface of each ovary of group 3 showed four to five spherical small luteal VPs (diameter 1.2–1.4 cm) (Fig. 4B, C). Straight small terminal arterioles (diameter, 30–40 μm) supplied the luteal VPs. A dense and intricate capillary network, originating from these arterioles, penetrated and partially filled the luteal VP, as